Geophys. J. Int. (1995) **122,** 765–775

Geophysical analysis of zonal tidal signals in length of day

Benjamin Fong Chao,[1] James B. Merriam[2] and Yoshiaki Tamura[3]

[1] *Geodynamics Branch, NASA Goddard Space Flight Center, Greenbelt,* MD 20771, *USA*
[2] *Department of Geological Sciences, University of Saskatchewan, Saskatoon, Canada, S7N 0W0*
[3] *National Astronomical Observatory, Mizusawa, Iwate, Japan*

Accepted 1994 November 24. Received 1994 April 5

SUMMARY

The Earth's zonal response coefficient κ is estimated from the tidal signals in the observed length-of-day (LOD) data. Its magnitude and phase are functionals of the Earth's internal structure and dynamics. In this paper, an analysis of 13 years of precise LOD data (1980–1992) reveals strong signals for nine zonal tidal groups ranging from 5 to 35 days in period. Numerical estimates of κ for 27 major tides are thus obtained, 11 among which are considered sufficiently high in signal-to-noise ratio to provide meaningful geophysical constraints on the Earth's rotational dynamics. The results favour a κ magnitude close to, but somewhat smaller than, 0.315, which is the theoretical value for an elastic mantle completely decoupled from the fluid core plus equilibrium oceans. A small amount of dispersion is also detectable, where shorter periods tend to have lower κ magnitude and larger phase lag. Our κ magnitude estimates are consistent with two recently published non-equilibrium ocean-tide models and an anelastic response in the mantle, although an equilibrium response in the ocean and a purely elastic response in the mantle is not disallowed. Phase lags of a few degrees are required by both ocean-tide models, and by our data.

Key words: Earth's rotation, length of day, ocean tides, solid tides.

1 INTRODUCTION

The rotational speed of the solid earth varies slightly with time, causing variations in the length of day (LOD). Precise measurements of LOD in the last three decades have revealed variations on time-scales ranging from decadal, interannual, seasonal, intraseasonal, down to days and (recently) sub-daily. Apart from a secular 'braking' (e.g. Lambeck 1980) and small semidiurnal librations (Chao *et al.* 1991) due to external luni-solar tidal torques, LOD varies as a consequence of internal geophysical mass movements under the conservation of angular momentum. These mass movements occur in all components of the Earth: atmosphere, hydrosphere, solid mantle and fluid core.

In particular, as first pointed out by Jeffreys in 1928, LOD will change as a result of changes in the Earth's axial moment of inertia caused by zonal tidal deformations in the Earth. The amount of tidal deformation, under given forcing, depends on the Earth's physical structure and dynamical behaviour. The response of an elastic, spherically symmetric earth to external forcings is described by a set of transfer functions, namely Love numbers, which are dimensionless gross-Earth functionals. Among them only the second-degree zonal potential raised by the luni-solar tides is of concern here. Such a tidal potential induces a second-degree zonal response in a spherically symmetric earth; and only such response can affect LOD via conservation of angular momentum, as all other harmonics are 'orthogonal' to ΔLOD. The induced ΔLOD in an elastic, spherically symmetric earth is thus proportional to the second-degree zonal transfer function, or the Love number k_2.

The concept of the transfer function can be extended naturally to include other dynamic behaviour of the Earth in the geophysical excitation of ΔLOD. Called the zonal response coefficient κ (as a function of frequency ω) by Agnew & Farrell (1978), it is defined as the ratio of the fractional change in LOD to the prescribed second-degree zonal tidal potential normalized with respect to the Earth's surface gravitational potential:

$$\frac{\Delta\mathrm{LOD}(\omega)}{\mathrm{LOD}} = -\kappa(\omega)\frac{\sqrt{5}}{3\sqrt{\pi}}\frac{a^3}{GC}V_2(\omega), \tag{1}$$

where G is the gravitational constant, a is the Earth's mean radius and C its axial moment of inertia, and the prescribed tidal potential equals the tidal potential amplitude V_2 multiplied by the fully normalized surface spherical harmonic Y_{20}.

If the Earth were entirely elastic, then its κ would be identical to the (static) k_2. This can be seen from the

conservation of angular momentum and MacCullagh's formula, assuming zero change in the trace of the inertia tensor (Rochester & Smylie 1974). The value of k_2 can be computed according to elastic, spherically symmetric earth models, and is found to be not very sensitive to model differences. In this paper we shall adopt a constant $k_2 = 0.300$ [which is the average of 0.299 by Wahr, Sasao & Smith (1981) and 0.301 by Smith & Dahlen (1981), both based on the 1066A earth model of Gilbert & Dziewonski (1975)]. However, the presence of the oceans, the fluid core, and anelasticity in the mantle combine to make κ differ from 0.300. Model computations show that the tidal deformation of an equilibrium ocean would increase the magnitude of κ by some 16 per cent (Agnew & Farrell 1978; Merriam 1980), whereas a complete decoupling of the fluid core from the mantle in ΔLOD excitation would reduce κ by about 11 per cent (Merriam 1980; Yoder, Williams & Parke 1981; Wahr *et al.* 1981). Such an idealized earth model would then have $\kappa = 0.315$. This value will be used below as a reference 'baseline'.

The real Earth deviates somewhat from this idealized baseline state; it is this deviation that is of particular geophysical interest here. The ocean tides are known to deviate from equilibrium, and the strength of the core–mantle (de)coupling depends on the forcing mechanism under the time-scale in question. These facts will introduce frequency dependence, or dispersion, in κ as explicitly indicated in eq. (1). Furthermore, κ becomes complex-valued due to tidal energy dissipation occurring in the ocean, mantle and core. The associated (non-zero) phase lag is a measure of the rate of this dissipation. Thus, observations of $\kappa(\omega)$ in magnitude and phase would provide important information towards the understanding of the dynamic properties of the Earth.

Groundwork has been laid and important progress has been made on this line of study, notably by Angew & Farrell (1978), Merriam (1980), Yoder *et al.* (1981), Wahr *et al.* (1981), Luo *et al.* (1987), Hefty & Capitaine (1990), Nam & Dickman (1990), McCarthy & Luzum (1993) and Robertson, Ray & Carter (1994). A major obstacle, nevertheless, has been the large uncertainties in the estimates of the tidal signals in LOD. The present paper re-examines this problem. We present a new set of estimates, both of the magnitude and the phase lag of the tidal signals based on modern LOD data. We analyse 13 years of LOD data, 1980–1992, for 27 zonal tides with periods ranging from 5 to 35 days. Among these, the 11 tides with the highest signal-to-noise ratios are selected for further geophysical study.

2 DATA ANALYSIS

The LOD data that we use are derived from the 'Space92' universal time (UT1) series (Gross 1993a), spanning 13 years from 1980 January 1.0 (at 0000Z, or midnight Greenwich Mean Time), to 1992 December 31.0. The Space92 UT1 data are the result of a Kalman filter combination of all the available space geodetic measurements of Earth orientation (where the zonal tidal signals are retained); they are given at nominal daily intervals. Since 1985, the observational data that has gone into the combined solution has included daily measurements. Prior to that the more typical sampling interval was 3 to 5 days. Subdaily fluctuations are to some extent averaged out, and major diurnal and semidiurnal tidal terms further removed according to a model as given in Herring & Dong (1994). Any remaining aliasing is believed to be negligible.

The LOD is obtained by a simple day-to-day differencing of UT1 data. A linear interpolation and resampling is subsequently applied to bring the nominal sampling back to 0000Z. Fig. 1(a) shows the ΔLOD time series in units of milliseconds (ms). The mean value has been removed. We precluded pre-1980 data because of their poorer quality and generally less frequent observations. We choose, however, to use as long a timespan T as feasible, in order to take advantage of the 'processing gain', that is, the $\sqrt{T}$ increase in the signal-to-noise ratio (SNR) for harmonic functions. Higher values of the SNR yield smaller uncertainties in the estimates (see eq. 3 below).

Another crucial benefit of the higher SNR is in resolving spectral lines that are close in frequency. In Fourier analysis of random signals, frequency resolution is nominally limited by the inverse of T. For coherent functions (such as tides), however, resolutions higher than $1/T$ ('super-resolution') are readily achievable. As an extreme example, imagine a time series consisting of two sinusoids of known frequencies recorded with infinite percision and zero noise. Then, obviously, only four points of the time series are required to solve for these two sinusoids analytically, no matter how close the two frequencies are, or how these four points are sampled in time. In reality, the resolving power is dependent upon the SNR, as demonstrated by Munk & Hasselmann (1964), and hence not limited by $1/T$ as long as the SNR is sufficiently high. In our analysis below, tidal terms separated by 1/(18.6 years) are well separated using just 13 years of data.

Figure 1(b) displays the power spectrum of ΔLOD of Fig. 1(a). The spectrum is computed using the multitaper technique of Thomson (1982), which provides robust and minimum-leakage spectral estimates. Seven orthogonal tapers with the time-bandwidth product of 4π were adopted in the computation. The rectangular shape of the spectral peaks is characteristic of a multitaper spectrum. The power spectrum shows the peaks of eight major tidal groups, as well as the decadal and seasonal signals above a red background. Within each tidal group the individual components are not visibly resolvable. The red background originates primarily from the ΔLOD signal caused by the variation in the atmospheric angular momentum (AAM).

Recognizing this, our data analysis consists of two stages of least-squares fit performed on the ΔLOD time series. The first fit is an interim one, and the goal is to yield a 'clean' tidal series by removing non-tidal excitation sources. To do this we model the ΔLOD time series as a linear combination of the major excitation terms:

$$\begin{aligned}\Delta\text{LOD} = {} & \text{decadal term} + 3\ \text{seasonal terms} \\ & + \text{AAM} + 27\ \text{zonal tide terms} \\ & + \text{un-modelled noise.}\end{aligned} \tag{2}$$

The decadal term in (2) is empirically chosen to be a sixth-degree polynomial. It accounts for the slow undulation (and the mean value) in ΔLOD, even though the geophysical origin of this undulation is presently uncertain.

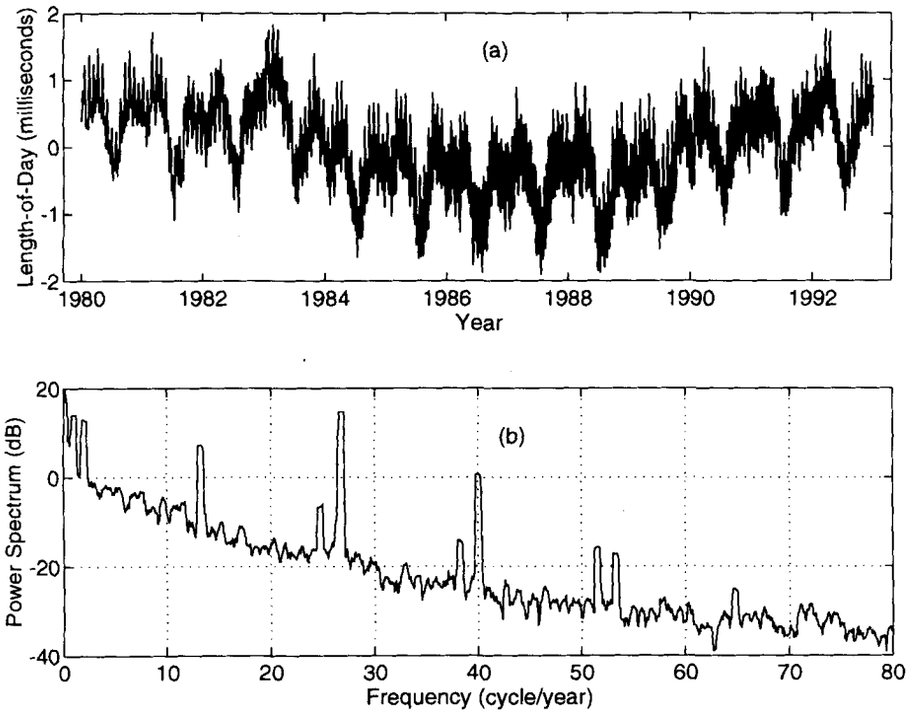

Figure 1. (a) The daily ΔLOD time series used in this study, from 1980 January 1.0 to 1992 December 31.0. A mean value has been removed. (b) Its multitaper power spectrum in the frequency range of 0–80 cycles per year, showing strong tidal and seasonal signals superimposed on a red background due to AAM.

The three seasonal terms in (2) are annual, semi-annual, and terannual. Although, as is well known, AAM explains most of the observed seasonal variation in ΔLOD, other contributions such as oceanic angular momentum, continental water storage and solid tides are all present in ΔLOD at seasonal periods. The seasonal terms are included here to account for these contributions. The seasonal and tidal terms are each represented by a sine wave plus a cosine wave.

The AAM variation is known to be a major, wide-band source for ΔLOD excitation (e.g. Barnes *et al.* 1983; Rosen, Salstein & Wood 1990; Hide & Dickey 1991). Removing it makes a decisive difference (and improvement) in subsequent tidal estimates. For example, studies based on older UT1 data and without removing AAM often yield $\kappa(Mm) < \kappa(Mf)$, whereas more recent ones in which AAM is removed tend to conclude the opposite [see Nam & Dickman (1990) for a summary].

We concatenate two AAM series to match the 13-year span of ΔLOD: the ECMWF (European Centre for Medium-range Weather Forecasts) AAM series prior to 1983 September 28.0, and the JMA (Japan Meteorological Agency) AAM data that has become available since that date. The AAM is the sum of the zonal wind term and the pressure term. The wind term is the dominant term in AAM and must be evaluated from global zonal wind speed at all altitudes. The ECMWF data cover altitude only up to the 100 mb level (encompassing 90 per cent of the mass of the atmosphere), while JMA covers up to 10 mb (99 per cent of the atmosphere). The JMA series furthermore appears to be more homogeneous over time, but has to be resampled (here by linear interpolation) to conform to our 0000Z daily sampling. There seems to be no discontinuity at the junction of the two sections after a mean has been removed from each section. The pressure term is relatively small. It is often evaluated under two idealized extremes: with or without the inverted-barometer (IB) effect. The IB is an idealized effect which assumes a complete and instantaneous isostatic response of the ocean water level to the changing barometric loading and unloading. The reality presumably lies somewhere in between the two extreme cases of IB and non-IB. Here we include both pressure terms (in addition to the wind term) in the AAM in eq. (2) for a determination of the optimal linear combination of them. This empirical procedure ensures the optimal removal of the AAM influence from ΔLOD.

The AAM series was further processed before fitting to eq. (2): it was moderately low-pass filtered at 50 cycles per year (cpy), for the following reasons. (i) Beyond about 50 cpy the AAM data are found to be poorly correlated with ΔLOD (e.g. Dickey *et al.* 1992). (ii) Our computed power spectra of AAM is somewhat less red than that of the ΔLOD used here (Fig. 1b). They coincide well at low frequencies, but the AAM power gradually exceeds the ΔLOD power towards the high-frequency portion of the spectrum at around 50 cpy. Therefore we low-pass filter the AAM series in order not to 'contaminate' ΔLOD (as AAM is later subtracted) at high frequencies where some of the tides reside.

The task now is to perform an optimal estimation of the first four sets of terms in eq. (2), with $(7 + 3 \times 2 + 3 + 27 \times 2) = 70$ parameters, so that the variance of the remaining un-modelled noise is minimized. This is achieved through a linear least-squares fit to (2). The result is used to subtract

the first three sets of terms. The residual series is then high-pass filtered with a zero-phase filter at the cut-off frequency of 2 cpy (see below for a reason). The result is called ΔLOD_T below (T for tide), shown in Fig. 2(a).

The multitaper power spectrum of ΔLOD_T is shown in Fig. 2(b). With a background spectrum much lower than that in Fig. 1(b), nine tidal groups (*cf.* Table 1) are clearly revealed. To demonstrate how 'clean' ΔLOD_T is, one can subtract the tidal estimate [the fourth term in (2)] from ΔLOD. One can then do yet another least-squares fit, on this difference, of the first three sets of terms in (2) and subsequently subtract these fits to yield our best estimate of the residual 'noise' series. The latter, together with its power spectrum (not shown), indeed show virtually no power left at the tidal frequencies. This residual time series also demonstrates the need for the high-pass filter to yield ΔLOD_T above: otherwise, a strong ~2-year undulation during the first 3.7 years would remain in ΔLOD_T, possibly having an adverse effect on our subsequent tidal fit. This undulation arises as a result of the exclusion of high-altitude wind data in the ECMWF data set used for the first 3.7 years in our AAM series: any stratospheric AAM, particularly that associated with the quasi-biennial oscillation (QBO), remains unaccounted for during that period. It is indeed found that the undulation matches virtually in entirety with the QBO AAM computed by Chao (1989).

Our tidal series ΔLOD_T is then used in a refined, second stage of least-squares fit, this time mainly for the 27 tidal terms, but the three seasonal terms were still included to absorb any seasonal power that might remain in ΔLOD_T. There are thus 60 parameters to be fitted, out of which 54 are targeted for our tidal components. Finally, the tidal ΔLOD estimates in terms of sine and cosine amplitudes are converted into the magnitude and phase. They are displayed in Table 1 and discussed in the next section.

Table 1. Estimates of κ magnitude and phase lag (in degrees) with their 1σ uncertainty, obtained from 11 zonal tidal signals in observed ΔLOD. The baseline is the theoretical tide amplitude predicted by a κ of 0.315, given here for reference.

Tide Period (day)	Baseline (μs)	Magnitude $\pm \sigma$ κ	Phase lag $\pm \sigma$ (°)
Msm: 31.8119	34.7749	0.3327 ± 0.041	-2.8 ± 7.5
Mm: 27.5546	181.8317	0.3081 ± 0.0067	0.4 ± 1.2
Msf: 14.7653	30.1588	0.3411 ± 0.024	10.0 ± 4.1
13.7773	14.9025	0.3027 ± 0.046	-2.2 ± 8.6
Mf: 13.6608	344.2066	0.3106 ± 0.0020	2.7 ± 0.4
Mf': 13.6334	142.7121	0.2981 ± 0.0048	5.1 ± 1.0
Mstm: 9.5569	12.5173	0.3263 ± 0.039	5.4 ± 7.9
Mtm: 9.1329	65.9026	0.3005 ± 0.0067	3.0 ± 1.3
9.1207	27.3182	0.3120 ± 0.016	5.3 ± 3.1
Msqm: 7.0958	10.5241	0.3037 ± 0.027	5.4 ± 6.0
Mqm: 6.8594	8.7205	0.3077 ± 0.032	-2.3 ± 6.7

3 RESULTS AND DISCUSSION

Our final results (Table 1) agree well with the theoretical baseline values, despite the large range in amplitude from several to several hundred microseconds (μs). The baseline

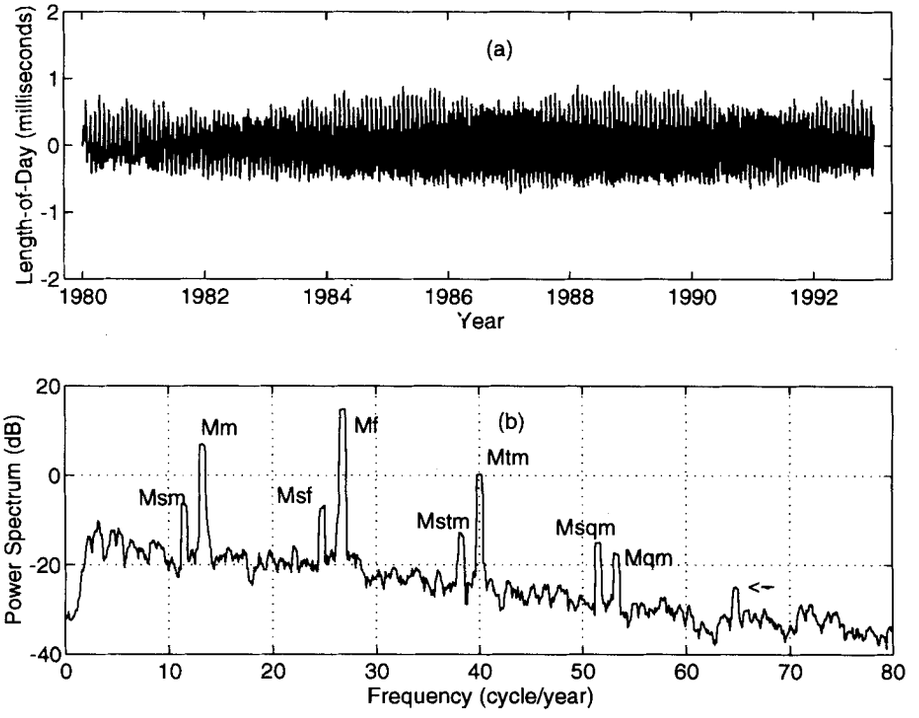

Figure 2. As Fig. 1, but for the 'clean' tidal signal (designated as ΔLOD_T in the text) extracted from ΔLOD by removing the decadal, interannual and seasonal variations as well as the (low-passed) AAM influence.

magnitude, as explained above, corresponds to a theoretical value of $\kappa = 0.315$, whereas the baseline phase is simply that of the prescribed tidal potential, all according to the tide table of Tamura (1993). The magnitude and phase are sometimes given in terms of the universal time (UT1), which represents the cumulative effect of ΔLOD in Earth orientation. To make the conversion to UT1, the amplitude in ΔLOD should be multiplied by the corresponding period in days divided by 2π, while the phase angle should be retarded by 90°.

It is the departure of the estimates from the baseline values that are of geophysical interest. Without error bounds, the estimates are by themselves of little geophysical use. The standard deviations (σ) of the estimate assuming zero-mean, white, additive noise can be evaluated according to the following formula from Chao & Gilbert (1980):

$$\frac{\sigma(\text{amplitude})}{\text{amplitude}} = \sigma(\text{phase}) = \frac{1}{\sqrt{2}\,\text{SNR}}, \quad (3)$$

where the phase is in radians, and SNR is the signal-to-noise ratio for spectral amplitude of a harmonic function in the frequency domain. To evaluate the SNR, we take the baseline value as the signal amplitude, while the noise amplitude is read off the envelope of the background noise spectrum from Fig. 2(b) (with proper conversion in units).

We present the final estimates in Table 1. Columns 1 and 2 give the period of the tides in (solar) days and the baseline tidal amplitude in ΔLOD (based on $\kappa = 0.315$). Our tidal amplitude estimates are converted into equivalent κ magnitude (equation 1) and given in Column 3 with the 1σ uncertainty (eq. 3). Column 4 gives the corresponding phase-lag estimates (with respect to baseline phase), also with the 1σ uncertainty. Table 1 only lists the estimates of the κ magnitude and phase lag for the 11 (out of 27) tides that have the highest SNR: $\sigma(\text{magnitude}) < 0.005$ and $\sigma(\text{phase}) < 10°$. They are plotted in Fig. 3, relative to the baseline values.

3.1 The non-equilibrium oceans and core–mantle decoupling

Since the equilibrium ocean tide has such a large influence on κ it is worthwhile to examine the consequences of a non-equilibrium tide. The long-period ocean tides are known to depart from equilibrium. Miller, Luther & Hendershott (1993) and Cartwright & Ray (1990) summarize the character of the *Mm* and *Mf* tides. Amplitudes are close to equilibrium, but they may slightly exceed equilibrium in the tropics and they are a little smaller than equilibrium at mid-latitudes. At high southern latitudes they are below equilibrium, and at high northern latitudes they are greater than equilibrium. Their phase leads the equilibrium tide at high latitudes, and lags the equilibrium at low and mid-latitudes. Most of the axial angular momentum of the tide is at low latitudes, so the character of the tide at low latitudes controls its effect on LOD. This means that the dynamic tide ΔLOD signal should then lag the equilibrium. Since the ocean contributes about 16 per cent to κ, and the lag of the dynamic tide in the tropics is about 20°, the lag of κ should be about 3°. This is what is observed.

The equilibrium ocean makes a contribution to ΔLOD only through the change in its inertia tensor (the relative angular momentum, i.e. the 'motion term', due to equilibrium tidal currents in the axial angular momentum vanishes). In the dynamic tide, a westward current is raised in the tropics as a result of conservation of angular momentum acting on the equatorial bulge of the zonal tides. This current results in a small decrease in the in-phase amplitude of the total angular momentum. The phase lag in the tropical ocean seems to be the result of the propagation time of a gravity wave from the strongly excited Arctic ocean to the tropical Pacific (Miller *et al.* 1993). Friction further increases the phase lag by slowing the propagation of these gravity waves, so that friction has the somewhat counter-intuitive effect of driving the tide further from equilibrium. The net effect on κ is a small decrease in the in-phase part, and the creation of an out-of-phase part of about the same magnitude as the decrease in the in-phase part.

Seiler (1991) has recently computed the total angular momentum of the *Mm, Mf,* and *Mf'* tides based on the tide model used previously by Brosche *et al.* (1989). Dickman (1993) has computed the effect on UT1 of the total angular momentum involved in seven long-period tides obtained by a spherical harmonic theory. Table 2 shows the long-period effects on UT1 calculated by Dickman (1993) and by Gross (1993b) using the total angular momentum of Seiler (1991). In both cases, the effect on UT1 is computed assuming a complete decoupling of the core from the mantle.

As explained above, $\kappa = 0.315$ for an equilibrium ocean response and a purely elastic mantle decoupled from the core. Merriam (1982) has shown how this is resolved into contributions from the solid earth and oceans:

$$\begin{aligned}\kappa &= \kappa_{\text{solid earth}} + \kappa_{\text{oceans}} \\ &= 0.268 + 0.048 = 0.315, \\ &\quad \text{with no core–mantle coupling} \\ &= 0.302 + 0.039 = 0.341, \\ &\quad \text{with perfect core–mantle coupling.}\end{aligned} \quad (4)$$

Note that core–mantle coupling has opposite effects on $\kappa_{\text{solid earth}}$ and κ_{oceans}: decreasing the amount of core–mantle coupling decreases $\kappa_{\text{solid earth}}$ but increases κ_{oceans}. This result somewhat masks the overall effect of core–mantle coupling on κ, but, since the effect on the solid earth dominates, there is an overall decrease in κ as the strength of core–mantle coupling decreases. Formulae (4) allow us to compare the κ that would be expected with any dynamic ocean tide. First we compute the UT1 signal with $\kappa = 0.268$, which is the solid earth value, and then we add the expected UT1 signal of the dynamic ocean model. The total is then normalized by the solid earth signal to give κ. The dynamic ocean UT1 signal depends on the angular momentum of the oceans and the degree of core–mantle coupling, but the range of this effect is small (the difference between a completely decoupled core and a perfectly coupled core is only 0.009 in κ_{oceans}). The evidence is so strongly in favour of a completely decoupled core (see also Chao 1994) that we can safely assume complete core decoupling in the construction of a dynamic κ_{oceans}. Column 2 of Table 2 is the baseline UT1 signal expected with $\kappa = 0.315$. Using formulae (4), we obtain the UT1 signal expected on an oceanless earth (Column 3). Column 4 shows

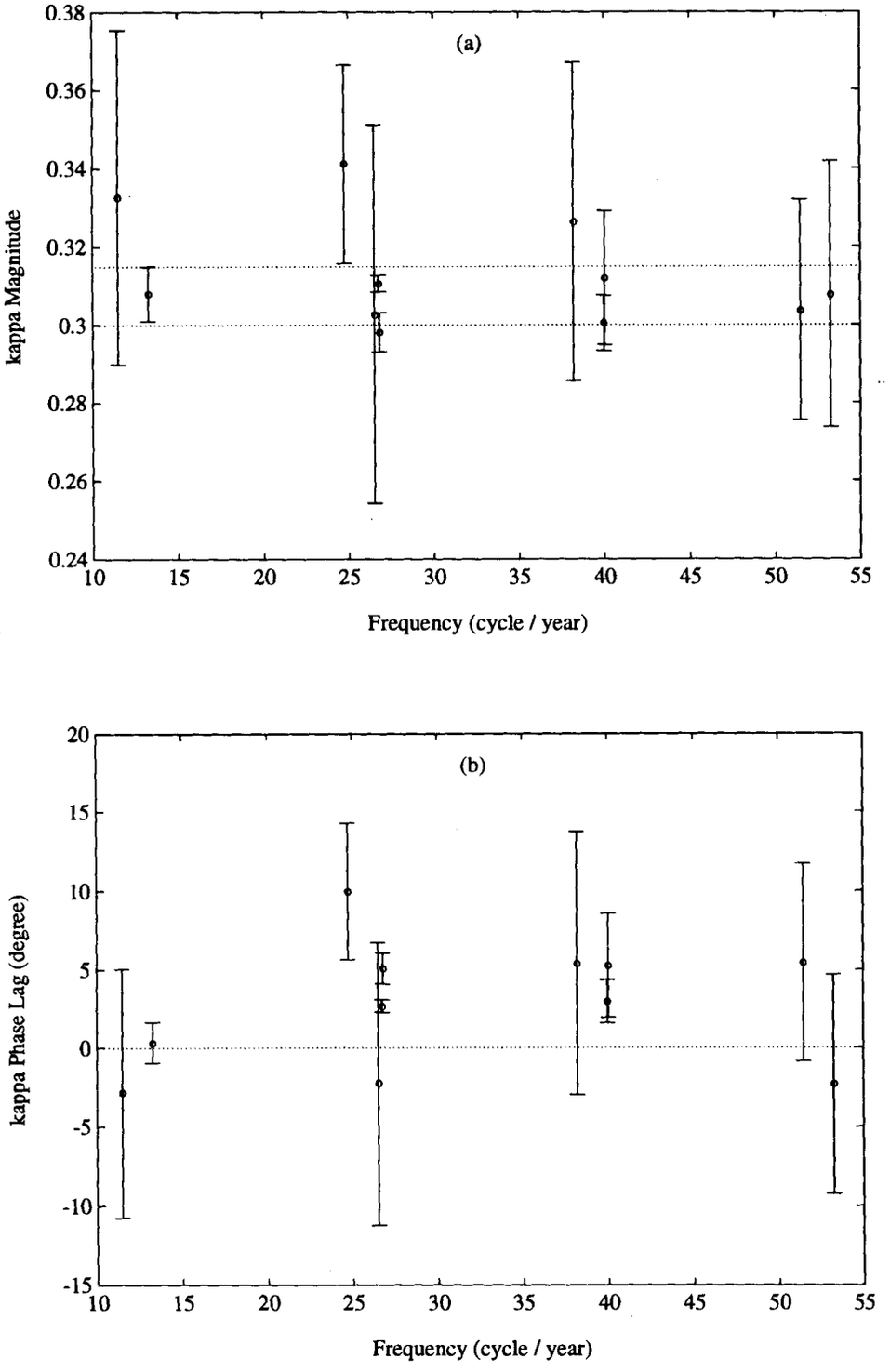

Figure 3. (a) 11 κ magnitude estimates whose 1σ uncertainties are less than 0.05, plotted (as O) against frequency. The dashed lines indicate the $\kappa = 0.315$ baseline and the static Love number $k_2 = 0.300$. (b) The corresponding 11 estimates for the κ phase lag whose 1σ uncertainties are less than 10°, relative to the zero baseline.

the (in-phase, out-of-phase) components of the dynamic oceans' contribution to UT1, from Dickman (1993) and Seiler (1991) models. Adding this to the oceanless earth value, we have, in Column 5, the total UT1 signal of the earth with dynamic oceans. This is then converted to κ magnitude (by normalizing with respect to period in Column 1 divided by 0.315) and phase lag, given in the last two columns.

Any frequency dependence of κ must come from core–mantle coupling, mantle anelasticity, or the ocean tides. Core–mantle coupling cannot be variable enough to amount to anything across the narrow zonal tide frequency

Table 2. The theoretically predicted κ assuming no core–mantle coupling and the dynamic ocean tides.

(1) Tide: Period (days)	(2) sin (μs)	(3) sin (μs)	(4) (sin, cos) (μs)	(5) (sin, cos) (μs)	(6) Magnitude κ	(7) Phase lag (°)
Mm: 31.8119	-184.8	-156.7	(-28.1, 2.4)	(-184.8, 2.4)	0.315	0.7
Mm: 27.5546	-837.3	-710.0	(-125.8, 11.0)	(-835.8, 11.0)	0.314	0.7
Msf: 14.7653	-74.4	-63.1	(-10.5, 1.8)	(-73.6, 1.8)	0.312	1.4
Mf: 13.6608	-785.8	-666.4	(-109.2, 21.2)	(-775.6, 21.2)	0.311	1.6
Mf': 13.6334	-325.7	-275.7	(-45.1, 8.8)	(-320.8, 8.8)	0.311	1.6
Mtm: 9.1329	-100.8	-85.5	(-12.4, 3.8)	(-97.9, 3.8)	0.305	2.2
9.1207	-41.6	-35.3	(-5.1, 1.5)	(-40.4, 1.5)	0.305	2.2
Mm: 27.5546	-837.3	-710.0	(-105.0, 25.3)	(-815.0, 25.3)	0.307	1.7
Mf: 13.6608	-785.8	-666.4	(-86.0, 35.0)	(-752.4, 35.0)	0.302	2.7
Mf': 13.6334	-325.1	-275.7	(-35.6, 14.5)	(-311.3, 14.5)	0.302	2.7

band considered here, and we will show that anelastic effects are also nearly constant across this band. This leaves a frequency-dependent ocean tide admittance as the only reasonable cause for the frequency dependence of κ, within this band. The ocean response to tidal forcing is known to be a slowly varying function of frequency (Platzman 1984). In other gross measurements of tidal response, for example tidal loading in gravity observations, the loading signal has a smooth, almost linear variation with frequency across the entire diurnal and semidurnal bands (Merriam 1995). Since dynamics are much less important in the long-period band in comparison, there is even more reason to expect a small frequency dependence in this band. Indeed, the evidence from our measurements, and from the tide models of Dickman and Seiler, suggests that this is so. There are known non-linear tides at *Mm* (resulting from an interaction between M_2 and N_2), at *Msf* (M_2 and S_2), and at *Mf* (K_1 and O_1), but these are small and likely to be local, shallow-water effects, which should average out of a global parameter such as κ. Thus, it is reasonable to expect the frequency dependence of κ to be so weak over the zonal tide frequency band as to appear nearly linear. Figs 4(a) and (b) show our measurements of the magnitude and phase lag of κ, respectively, with a weighted least-squares fit to a straight line. The 1σ envelopes on the best-fitting line are shown as dashed lines.

Also shown in Fig. 4 are the predictions of κ based on the theoretical tide models of Dickman and Seiler, which have only seven and three constituents respectively. They have therefore been linearly extended to cover the range of the 11 tides measured well here. The seven Dickman models fall nearly on a straight line, which supports our earlier contention. The three Seiler tides are too close together in frequency to draw any conclusions with regard to linearity, but the slope of the fit to these three agrees well with that of the Dickman model.

Both ocean tide models are in excellent agreement with our measurements on the frequency dependence of κ, in magnitude and in phase. The Dickman model is in better agreement with our results in magnitude, but in somewhat poorer agreement in phase than the Seiler model. It appears to underpredict the phase lag by about 1.5° on average, implying a tropical phase lag that is too small by about 10°. The linear frequency dependence of the phase for the Seiler model is in excellent agreement with our measurements. The linear fit for Seiler's magnitude is within 1σ uncertainty of ours, but its mean is lower than the mean of ours by about 0.008. Since the total ocean effect on κ is about 0.05, the disagreement in the mean is only one-sixth of the ocean tidal effect, which amounts to no more than 2 mm in the equatorial region.

If we accept that the difference in κ_{ocean} between the Seiler and Dickman results is a measure of the uncertainty in both, then both models are compatible with our data. The differences in magnitude between our measurements and either tide model are easily explained by model uncertainties—no ocean tide model is good to much better than 1 mm, which is the difference between our measurements and the tide models.

3.2 Mantle anelasticity

Wahr & Bergen (1986, henceforth WB) have predicted the effects of anelasticity on the Love number k_2 at *Mm* and *Mf* in the frequency band we examine here. These may be summarized by saying that anelasticity increases the magnitude and delays the phase. Both effects decrease with frequency. If we assume that the effect of anelasticity on k_2 scales to its effect on κ the same way as k_2 scales to κ, that is, if $\Delta\kappa \approx 0.85\ \Delta k_2$, then we can obtain an estimate for κ with non-equilibrium oceans and anelasticity in the mantle. This procedure makes some simplifying approximations, but since the effect of anelasticity is small to begin with, the approximations should be adequate. In passing we note that

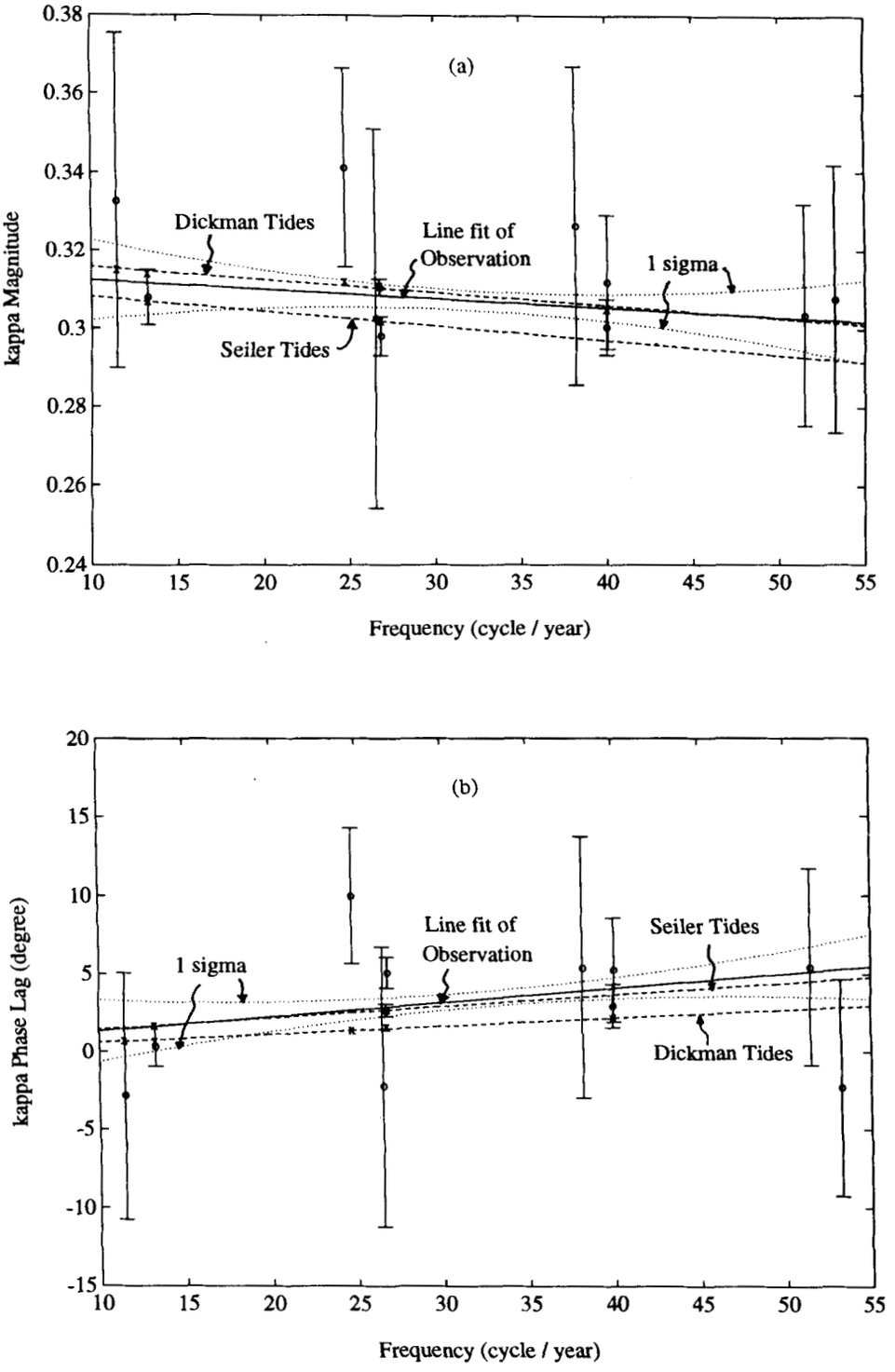

Figure 4. The 11 estimates in Fig. 3 compared with model predictions. The solid line is a weighted least-squares fit of a straight line to our estimates, the dotted lines are the 1σ uncertainty envelopes on the fitted line. The predicted κ magnitude with the Dickman (1993) and Seiler (1991) ocean tides are shown (as $\times$), linearly extended (dashed lines) to span the frequency band considered here. (a) For the κ magnitude; (b) for the κ phase lag.

the ocean tide models of Dickman already accommodate mantle anelasticity. By this procedure, we derive the results in Table 3. The lines labeled *Mm* and *Mf* are the predicted anelastic κ based on $\kappa = 0.315$ and the lower/upper bounds of WB. The line labelled Range is the range of the anelastic effect on κ extrapolated over the entire zonal tide band considered here. The line labelled Mean is the mean value of the predicted anelastic effect, in the centre of this band.

It can be seen that the frequency dependence of anelasticity is small, amounting to a decrease in magnitude

Table 3. The lower and upper bounds on κ, with the anelastic earth models of k_2 from Wahr & Bergen (1986).

	Lower Bound		Upper Bound	
	mag.	phase(°)	mag.	phase(°)
Mm (27.5546 d)	0.318	0.1	0.330	0.6
Mf (13.6608 d)	0.318	0.1	0.330	0.6
Range	0.001	0.01	0.004	0.0
Mean	0.003	0.1	0.015	0.6

of 0.001 and an increase in phase lag of 0.01° with frequency across the zonal tide band. These are much smaller than the uncertainty on the linear change of our own measurements. When our measurements are corrected for either the Dickman or Seiler tide models, the resulting magnitude is almost independent of frequency, although small positive and negative frequency dependences of much larger magnitude than the WB predictions suggest are admissible at the 1σ level. The corrected phases show a slight increase in the lag with frequency when either tide model is used, but a decrease with frequency is also admissible at the 1σ level. The frequency band in consideration is simply too narrow to allow a reasonable constraint to be put on anelastic effects.

The elastic mantle contribution to κ is nominally calculated at seismic frequencies as the earth model used to generate this value is derived from seismic data. The increase in κ from seismic frequencies to the zonal tide band is 0.005 for the WB lower bound, and 0.015 for the upper bound, so the bounds on the predicted κ for an equilibrium ocean are then 0.320 and 0.330 in magnitude, and 0.1° and 0.6° in phase. For the dynamic ocean tides the predicted κ when anelasticity is included can be estimated by simply adding uniform shifts to the predicted dynamic tide κ in Fig. 4, and increasing the frequency dependence slightly. The range of uncertainty in the predicted κ now includes the range of uncertainty in the ocean tide models and that of the WB anelastic earth models. Our results, shown in Fig. 5, and summarized below, are consistent with the range of anelastic models represented by the WB lower/upper limits.

The shaded area in Fig. 5 is the 1σ confidence interval on a weighted least-squares fit of a straight line to our measurements (same as in Fig. 4). The solid lines are the extreme range of the magnitude and phase of κ implied by the uncertainties in the ocean tide models plus the lower/upper limits of the WB anelastic response. The combination of the Dickman tides and the WB upper limit provides the extreme upper bound on predicted κ magnitude (Fig. 5a), while the combination of the Seiler

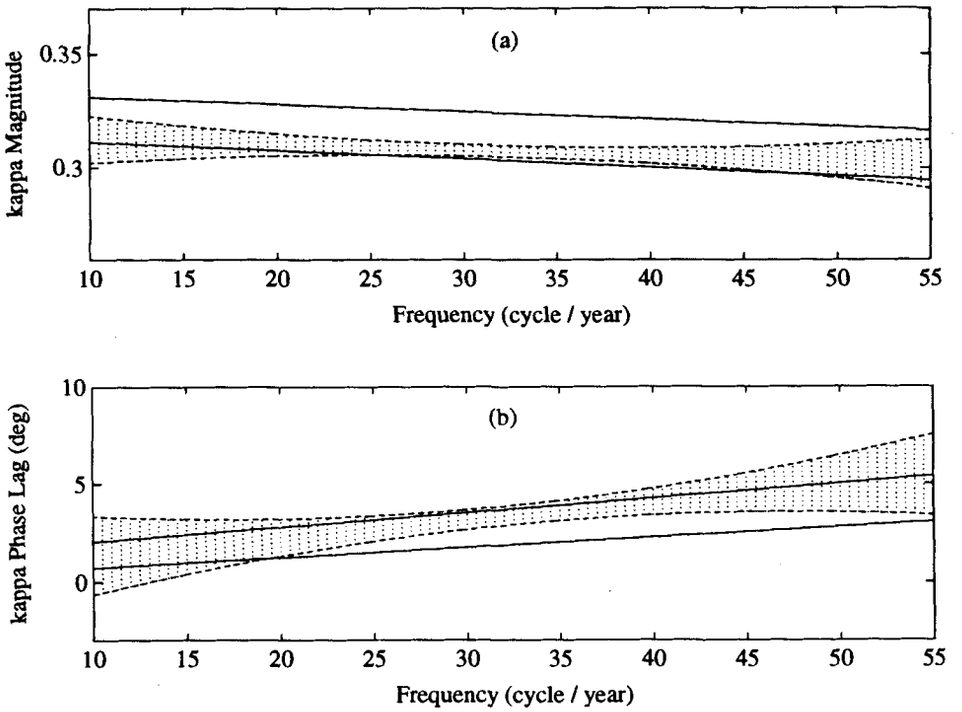

Figure 5. (a) The shaded area is the 1σ confidence interval (same as Fig. 4) on a weighted least-squares linear fit to observed κ magnitude with frequency. The solid lines are the extreme lower/upper bounds on the predicted κ magnitude using Dickman (1993) and Seiler (1991) tides and the Wahr & Bergen (1986) bounds on anelasticity. (b) Same for the phase lag of κ.

tides and the WB lower limit gives the extreme lower bound on κ magnitude. The combination of the Seiler tides and the WB upper limit provides the extreme upper bound on the phase lag (Fig. 5b), and the combination of Dickman tides and the WB lower limit gives the extreme lower bound on the phase lag. It should be noted that most of the range between the extreme lower and upper bounds reflects the uncertainty in the ocean tide. This means that a more stringent observational constraint on anelasticity in the mantle awaits an improvement in ocean tide models.

4 SUMMARY AND CONCLUSIONS

We have measured the magnitude and phase of the zonal response coefficient κ for 27 zonal tides in the long-period band from 5 to 35 days. Of these, we have selected the 11 with the smallest uncertainties for further analysis. The magnitude estimates are found to favour strongly a complete decoupling of the core from the mantle within this band. By arguing on reasonable grounds that the largest frequency dependence within the band should be due to the ocean tide admittance, and further that the band is too narrow and the frequency dependence of the ocean tide admittance so benign, the frequency dependence in κ should be almost linear across this band. We then placed limits on the frequency dependence in magnitude and in phase lag. These have been shown to be due to the departure of the ocean tide from equilibrium as demonstrated in recent tide models. We have also found that our results are consistent with the range of anelastic models of the mantle. A tighter constraint on mantle anelasticity awaits improvements in ocean tide models.

ACKNOWLEDGMENTS

We are indebted to the following colleagues for providing necessary data used in this work: R. Gross for the Space92 series, I. Naito for the JMA AAM data, and ECMWF and A. Au for the ECMWF AAM data. We also thank T. Sasao for insightful discussions. This work is supported by the NASA Geophysics Program, the Natural Sciences and Engineering Research Council of Canada, the Japan Society for the Promotion of Science, and the Japanese National Astronomical Observatory Visiting Fellowship Program.

REFERENCES

Agnew, D.C. & Farrell, W.E., 1978. Self-consistent equilibrium ocean tides, *Geophys. J. R. astr. Soc.*, **55,** 171–181.

Barnes, R.T.H., Hide, R., White, A.A. & Wilson, C.A., 1983. Atmospheric angular momentum fluctuations, length-of-day changes and polar motion, *Proc. R. Soc. Lond.*, **A387,** 31–73.

Brosche, P., Seiler, U., Sündermann, J. & Wünsch, J., 1989. Periodic changes in Earth's rotation due to oceanic tides, *Astron. Astrophys.*, **220,** 318–320.

Cartwright, D.E. & Ray, R.D., 1990. Observations of *Mf* ocean tide from Geosat altimetry, *Geophys. Res. Lett.*, **17,** 619–622.

Chao, B.F., 1989. Length-of-day variations caused by El Niño–Southern Oscillation and Quasi-Biennial Oscillation, *Science*, **243,** 923–925.

Chao, B.F., 1994. Transfer function for length-of-day variations: Inference for Earth dynamics, *EOS, Trans. Am. geophys. Un.*, **75,** 111.

Chao, B.F. & Gilbert, F., 1980. Autoregressive estimation of complex eigenfrequencies in low frequency seismic spectra, *Geophys. J. R. astr. Soc.*, **63,** 641–657.

Chao, B.F., Dong, D.N., Liu, H.S. & Herring, T.A., 1991. Libration in the Earth's rotation, *Geophys. Res. Lett.*, **18,** 2007–2010.

Dickey, J.O., Marcus, S.L., Steppe, J.A. & Hide, R., 1992. The Earth's angular momentum budget on subseasonal time scales, *Science*, **225,** 321–324.

Dickman, S.R., 1993. Dynamic ocean-tide effects on Earth rotation, *Geophys. J. Int.*, **112,** 448–470.

Gilbert, F. & Dziewonski, A.M., 1975. An application of normal mode theory to the retrieval of structural parameters and source mechanisms from seismic spectra, *Phil. Trans. R. Soc. Lond.*, **A278,** 187–269.

Gross, R.S., 1993a. A combination of Earth orientation data: Space92, *IERS Tech. Note* **14,** Observatoire de Paris.

Gross, R.S., 1993b. The effect of ocean tides on the Earth's rotation as predicted by the results of an ocean tide model, *Geophys. Res. Lett.*, **20,** 293–296.

Hefty, J. & Capitaine, N., 1990. The fortnightly and monthly zonal tides in the Earth's rotation from 1962 to 1988, *Geophys. J. Int.*, **103,** 219–231.

Herring, T.A. & Dong, D., 1994. Measurement of diurnal and semidiurnal rotation variations and tidal parameters of the Earth, *J. geophys. Res.*, **99,** 18 051–18 071.

Hide, R. & Dickey, J.O., 1991. Earth's variable rotation, *Science*, **253,** 629–637.

Lambeck, K., 1980. *The Earth's Variable Rotation*, Cambridge University Press, New York.

Luo, S., Zheng, D., Robertson, D.S. & Carter, W.E., 1987. Short-period variations in length of day: Atmospheric angular momentum and tidal components, *J. geophys. Res.*, **92,** 11 657–11 661.

McCarthy, D.D. & Luzum, B.J., 1993. An analysis of tidal variations in the length of day, *Geophys. J. Int.*, **114,** 341–346.

Merriam, J.B., 1980. Zonal tides and changes in the length of day, *Geophys. J. R. astr. Soc.*, **62,** 551–561.

Merriam, J.B., 1982. A comparison of recent theoretical results on the short-period terms in the length of day, *Geophys. J. R. astr. Soc.*, **69,** 837–840.

Merriam, J.B., 1995. Non-linear tides observed with the superconducting gravimeter at Cantley, Quebec, *Geophys. J. Int.*, in press.

Miller, A.J., Luther, D.S. & Hendershott, M.C., 1993. The fortnightly and monthly tides: Resonant Rosby waves or nearly equilibrium gravity waves? *J. Phys. Oceanog.*, **23,** 879–897.

Munk, W. & Hasselmann, K., 1964. Super-resolution of tides in *Studies on Oceanography*, pp 339–344 Hidaka Memorial Volume, Univ. of Washington Press, Tokyo.

Nam, Y.S. & Dickman, S.R., 1990. Effects of dynamic long-period ocean tides on changes in Earth's rotation rate, *J. geophys. Res.*, **95,** 6751–6757.

Platzman, G.W., 1984. Normal modes of the world ocean, Part IV: Synthesis of diurnal and semidiurnal tides, *J. Phys. Oceanog.*, **14,** 1532–1550.

Robertson, D.S., Ray, J.R. & Carter, W.E., 1994. Tidal variations in UT1 observed with very long baseline interferometry, *J. Geophys. Res.*, **99,** 621–636.

Rochester, M.G. & Smylie, D.E., 1974. On changes in the trace of the Earth's inertia tensor, *J. geophys. Res.*, **79,** 4948–4951.

Rosen, R.D., Salstein, D.A. & Wood, T.M., 1990. Discrepancies in the Earth-atmosphere angular momentum budget, *J. geophys. Res.*, **95,** 265–270.

Seiler, U., 1991. Periodic changes of the angular momentum budget due to the tides of the world ocean, *J. geophys. Res.*, **96,** 10 287–10 300.

Smith, M.L. & Dahlen, F.A., 1981. The period and Q of the

Chandler wobble, *Geophys. J. R. astr. Soc.*, **64,** 223–281.

Tamura, Y., 1993. Periodic series of ΔUT1, in *Proc. 7th IAG Int. Symp. no. 112,* pp. 435–438, eds Montag, H. & Reigber, C., Springer-Verlag, Berlin.

Thompson, D.J., 1982. Spectrum estimation and harmonic analysis, *Proc. IEEE,* **70,** 1055–1096.

Wahr, J.M. & Bergen, Z., 1986. The effects of mantle anelasticity on mutations, earth tides, and tidal variations in rotation rate, *Geophys. J. R. astr. Soc.*, **87,** 633–668(NB).

Wahr, J.M., Sadao, T. & Smith, M.L., 1981. Effect of the fluid core on changes in the length of day due to long period tides, *Geophys. J. R. astr. Soc.*, **64,** 635–650.

Yoder, C.F., Williams, J.G. & Parke, M.E., 1981. Tidal variations of Earth rotation, *J. geophys. Res.*, **86,** 881–889.